Accepted Manuscript

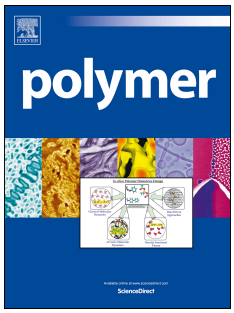

Synthesis and optoelectronic property manipulation of conjugated polymer photovoltaic materials based on benzo[*d*]-dithieno[3,2-b;2′,3′-*f*]azepine

Jian Wang, Pan Yin, Yue Wu, Gangjian Liu, Chaohua Cui, Ping Shen

PII: S0032-3861(18)30493-2

DOI: 10.1016/j.polymer.2018.06.007

Reference: JPOL 20644

To appear in: *Polymer*

Received Date: 25 January 2018

Revised Date: 14 April 2018

Accepted Date: 2 June 2018

Please cite this article as: Wang J, Yin P, Wu Y, Liu G, Cui C, Shen P, Synthesis and optoelectronic property manipulation of conjugated polymer photovoltaic materials based on benzo[*d*]-dithieno[3,2-b;2′,3′-*f*]azepine, *Polymer* (2018), doi: 10.1016/j.polymer.2018.06.007.

Graphical Abstract

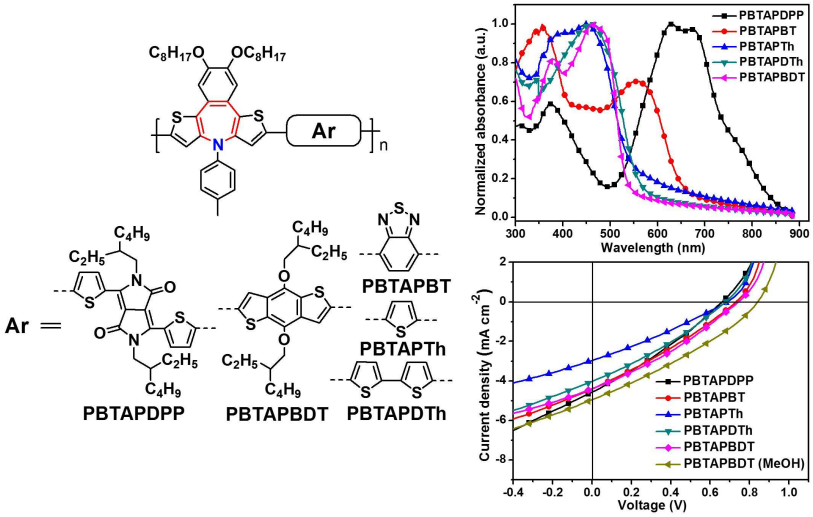

Synthesis and optoelectronic property manipulation of conjugated polymer photovoltaic materials based on benzo[*d*]-dithieno[3,2-*b*;2′,3′-*f*]azepine

Jian Wang[1], Pan Yin[1], Yue Wu[2], Gangjian Liu[1], Chaohua Cui[2], Ping Shen[1,*]

[1] Key Laboratory for Green Organic Synthesis and Application of Hunan Province, Key Laboratory of Environmentally Friendly Chemistry and Application of Ministry of Education, College of Chemistry, Xiangtan University, Xiangtan 411105, China

[2] Laboratory of Advanced Optoelectronic Materials, College of Chemistry, Chemical Engineering and Materials Science, Soochow University, Suzhou 215123, China

*Correspondence to: P. Shen (E-mail: shenping802002@163.com)

Abstract: To develop new conjugated polymers (CPs) based on heteroepines, a soluble azepine moiety of benzo[*d*]-dithieno[3,2-*b*;2′,3′-*f*]azepine was copolymerized with different building blocks to obtain a series of CPs. A broad absorption range of 300-850 nm and the desired optical bandgaps (1.54-2.42 eV) are easily accessible by varying different copolymerization units. The HOMO levels of polymers are observed as an almost identical value of -5.21 eV and the LUMO levels range from -2.82 to -3.52 eV. Polymer solar cells (PSCs) with these polymers as donor materials were fabricated to explore application potentials in organic photovoltaics. Preliminary study exhibits the best power conversion efficiency of 1.28% for PSCs based on these polymers with a relatively high V_{oc} of 0.84 V. Although photovoltaic performance of these new polymers is not as high as our expected, the first daring attempt provides some good references to expand application fields of azepine-based polymers.

Keywords: conjugated polymers; benzodithienoazepine; polymer solar cells

1. Introduction

Over the past two decades, conjugated polymers (CPs) have received continually increasing attention and been widely applied in polymer optoelectronic devices, such as polymer solar cells

(PSCs) [1-4], polymer light-emitting diodes (PLEDs) [5-7], polymer field effect transistors (PFETs) [8-10] and photodetectors [11,12], due to their intrinsic semiconducting characteristics. For CPs used in PSCs, strong and broad absorption ability, narrow bandgap, suitable molecular energy level, high and balanced charge carrier mobility are all of crucial importance for achieving excellent photovoltaic performance [13]. Additionally, another fundamental issue for designing high-performance PSCs is the control of the active layer morphology at the nanometer length scale, which also is of critical importance to the device efficiency [14-16]. The backbone of CPs is the most important component because it dominates most of the PSC-related optoelectronic properties mentioned above. The mainly reported conjugated backbones for PSC can be generally classified into two kinds based on the constitution of the repeating unit: homopolymer and copolymer. Hundreds of different backbones have been reported so far. Typical conjugated backbone is constructed by electron-rich and electron-deficient heteroarene units independently or together. The electron-rich benzo[1,2-*b*:4,5-*b′*]dithiophene (BDT) unit emerges as a most sparking tricyclic fused arene and has been widely used to build high-performance donor-donor (D-D) or donor-acceptor (D-A) type copolymers due to its symmetric, rigid and coplanar structure [1]. In 2008, Yang and Hou et al. reported a series of BDT-based D-D and D-A copolymers for the application of PSCs [17]. The results revealed that the optoelectronic properties, like absorbance, bandgap, molecular energy level, and charge carrier mobility, can be tailored effectively by copolymerizing with different electron-rich or electron-deficient units. Additionally, our group reported a series of photovoltaic copolymers based on 6,12-dihydro-diindeno[1,2-*b*;10,20-*e*]pyrazine (IPY) group, which is a multifused pentacyclic systems [18]. The bandgaps and molecular energy levels of the resulting IPY based CPs have also been controlled successfully by using the similar strategy. Expect for BDT and IPY, the other electron-rich multifused arenes, such as cyclopentadithiophene, indacenodithiophene, dithieno[2,3-*d*:2′,3′-*d*]benzo[1,2-*b*:4,5-*b′*]dithiophene units, are good building block for preparing efficiently photovoltaic polymers [19]. At present, it is very urgent to develop new multifused heteroarene unit because they could potentially yield novel photovoltaic polymers, and as a result that could contribute the further advance of power conversion efficiency (PCE) of PSCs.

In the past decades, conjugated seven-membered ring systems that have a heteroatom with a lone pair of electrons, denoted as heteroepines, have received a long-term interest due to their great

potential in molecular actuators and other mechanically responsive applications [20,21]. Among those heteroepines, nitrogen-containing azepine (**AP**, Chart 1) skeleton has attracted much attention because it is a peculiar structural motif in many biologically active and medicinally valuable molecules [22,23]. To improve thermal and electrochemical stability as well as drug activity, azepine usually is modified by the addition of annulation and steric effects. For example, benzene-annulated azepines (e.g. dibenz[*b*,*f*]azepine) and their derivatives have been variously proven as antiallergic activity, specifically antihistaminic activity, spansmolytic, serotonin antagonistic, fungicidal action, et al. [23]. In addition, T. M. Swager and co-workers reported the synthesis of thiophene-annulated azepine framework and its related conducting polymers [21]. The results demonstrated that the azepine-based polymers were thermally and electrochemically stable and retained their redox properties in the solid state, which could be applied in actuating materials research due to their redox stability and conductivity. Though annulated azepine-containing materials have shown great potential applications in molecular actuators and medicinally valuable molecules, there are a few limited examples about this kind of materials for applications in organic optoelectronic devices. For example, Ding [24] and Suh [25] groups reported on syntheses and photovoltaic applications of CPs containing an azepine-2,7-dione moiety. In addition, Su et al. synthesized a dibenz[*b*,*f*]azepine-containing sentistizer for dye-sensitized solar cell application [26].

Based on the above considerations, in this paper we present the design, synthesis, and characterization of a series of CPs based on a soluble and stable benzo[*d*]-dithieno[3,2-*b*;2′,3′-*f*]azepine (**BTAP**) unit (Chart 1), in which azepine unit is annulated with one benzene ring and two thiophenes to improve stability and structural modification of azepine building block. This paper is aimed at not only exploiting new azepine-based copolymers but also extending their application fields. Herein, three electron-rich donor units of thiophene (Th), dithiophene (DTh) and BDT and two electron-deficient acceptor building blocks of 2,1,3-benzothiadiazole (BT) and 3,6-dithiophen-2-yl-2,5-dihydropyrrolo[3,4-*c*]pyrrole-1,4-dione (DPP) were selected and copolymerized with annulated azepine motif (**BTAP**) to construct D-D (**PBTAPTh**, **PBTAPDTh**, and **PBTAPBDT**) or D-A (**PBTAPBT** and **PBTAPDPP**) copolymers as shown in Scheme 1. The thermal, optical, electrochemical, and charge carrier properties of these new copolymers were investigated systematically. Results indicated that the bandgap, molecular energy levels, and charge carrier mobility of azepine-based CPs can be fine manipulated by

selecting different copolymerizing units. Moreover, to tap the potential of optoelectronic devices, the initial photovoltaic performance of the new polymers were also investigated by preparing the PSC devices. Though photovoltaic performance of these new polymers is still poor so far, to the best of our knowledge, this is the first report on design, synthesis and characterization of benzo[*d*]-dithieno[3,2-*b*;2′,3′-*f*]azepine-based conjugated polymers for application in organic electronic devices. Our daring attempt provides some good references to expand application fields of azepine-based polymers and should also be useful for molecular structure design of other kinds of heteroepine-containing conjugated polymers serving in various optoelectronic devices.

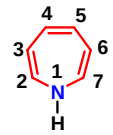

Azepine

(AP)

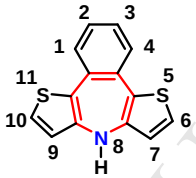

Benzo[*d*]-dithieno[3,2-*b*;2′,3′-*f*]azepine

(BTAP)

Chart 1. Molecular structures of azepine (**AP**) and benzo[*d*]-dithieno[3,2-*b*;2′,3′-*f*]azepine (**BTAP**) with relevant position numbered.

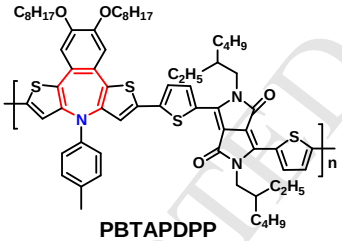

PBTAPDPP

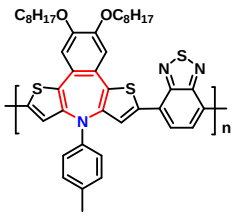

PBTAPBT

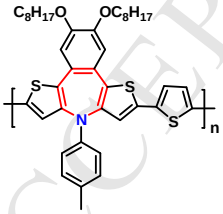

PBTAPTh

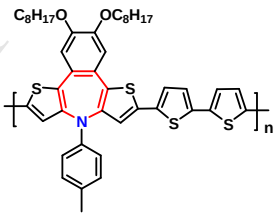

PBTAPDTh

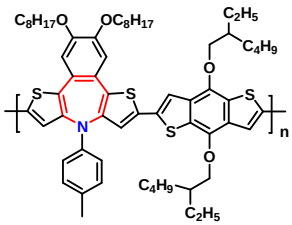

PBTAPBDT

Scheme 1. Chemical structures of **BTAP**-based copolymers.

2. Experimental section

2.1. Analytical instruments

Nuclear magnetic resonance (NMR) spectra were measured with Bruker AVANCE 400 spectrometer. Ultraviolet-visible (UV-Vis) absorption spectra were measured on PerkinElmer

Lamada 25 spectrometer. Molecular mass was determined by flight mass spectrometry (MALDITOF MS) using a Bruker Aupoflex-III mass spectrometer. Thermal gravimetric analysis (TGA) was performed under nitrogen at a heating rate of 20 °C min^{-1} with TGA Q50 analyzer. The molecular weight and polydispersity index (PDI) of the polymers were determined using Waters 1515 gel permeation chromatoraphy (GPC) analysis with tetrahydrofuran as the eluent and polystyrene as standard. The electrochemical cyclic voltammetry (CV) was recorded on a electrochemistry work station (CHI830B, Chenhua Shanghai) with a Pt slice electrode (coated with a polymer film), a Pt ring, and an Ag/AgCl electrode as the working electrode, the auxiliary electrode and the reference electrode respectively, in a 0.1 mol L^{-1} tetrabutylammonium hexafluorophosphate (Bu_4NPF_6) acetonitrile solution. Atomic force microscopy (AFM) measurement was carried out on a Digital Instruments (Bruker, Santa Barbara, CA, USA) using a tapping mode. Transmission electron microscopy (TEM) were performed on a JEM-2100 electron microscope operating at an acceleration voltage of 100 kV.

2.2. PSC device preparation and characterization

The solar cell devices were prepared with a architecture of ITO/PEDOT:PSS (30 nm)/active layer/Ca(20 nm)/Al(100 nm), where the active layer was comprised of the synthesized conjugated polymer as a donor and $PC_{61}BM$ or $PC_{71}BM$ as an acceptor. The indium tin oxide (ITO) patterned glass was cleaned with ultrasonic treatment in detergent, deionized water, acetone, ethanol, and isopropyl alcohol sequentially, and dried in an ultraviolet–ozone chamber for 15 min. A thin layer of PEDOT:PSS (~30 nm) was spin-coated on the pre-cleaned ITO glass at 5000 rpm and dried in an oven at 150 °C for 15 min subsequently. The polymer donor and the acceptor ($PC_{61}BM$ or $PC_{71}BM$) were dissolved in 1,2-dichlorobenzene (DCB) in different weight ratios and the total concentration of the donor/acceptor blending solution was 20 mg/mL. The solution was stirred at 100 °C for 6 h in a glovebox prior to use. The device was transferred to a glove box, where the above prepared blend solution was then spin-coated on PEDOT:PSS surface as the active layer. Subsequently, Ca (~20 nm) and Al (~100 nm) were successively evaporated on the top of the active layer under a vacuum of 5×10^{-4} Pa. The accurate device area was about 4 mm^2 as defined by shadow mask. The thicknesses of the active layer were controlled by varying the spin-coating speed and were measured on an Ambios Technology XP-2 surface profilometer. Photovoltaic performance of devices was tested under illumination condition with an AM 1.5G (100 mW cm^{-2}), and the current

density-voltage (*J-V*) characteristics were measured by a computer controlled Keithley 2602 Source Meter. The incident light intensity was calibrated using a standard Si solar cell. The hole mobility was measured by the space charge-limited current (SCLC) method with a hole-only device configuration (ITO/PEDOT:PSS/polymers:$PC_{71}BM$/MoO_3/Al) for hole mobility. Hole mobilities were extracted by fitting measured *J-V* curves using the empirical Mott–Gurney formula in single carrier SCLC device with the equation of $ln(JL^3/V^2) \approx 0.89(1/E_0)^{0.5} (V /L) + ln(9\varepsilon_0\varepsilon_r\mu/8)$.

2.3. Materials and synthesis

1,2-Benzenediol, 1-bromooctane, *p*-toluidine, thiophene, *N*-bromosuccinimide (NBS), tris(dibenzylideneacetone)dipalladium-chloroform adduct ($Pd_2(dba)_3 \cdot CHCl_3$), (t-Bu_3PH)BF_4, and tris(*o*-tolyl)phosphine (P(*o*-tol)$_3$), $Pd(PPh_3)_4$, *t*-BuONa and *n*-BuLi were purchased from J&K Chemical or Energy Chemical and used without further purification. Monomers **M2** and **M3** were purchased from Derthon (Shenzhen China) Optoelectronic Materials Science Technology Co., Ltd. Monomers **M4**-**M6** and 2-(tributylstannyl)thiophene were synthesized according to the published procedure [27,28]. The synthetic routes of **BTAP**-based monomer **M1** and the related polymers are outlined in Scheme 2 and Scheme 3, respectively. The synthetic procedure of other compounds are as follows.

*2.3.1. Synthesis of 1,2-dioctyloxybenzene (**1**)*

Under Ar protection, 1,2-benzenediol (5.5 g, 50 mmol), KOH (6.16 g, 110 mmol), and DMF (100 mL) were added into a 250 mL round bottom flask. The mixture was warmed up to 110 °C, then 1-bromooctane (21.2, 110 mmol) was added and the reaction mixture was continued to stir at this temperature for overnight. The mixture was cooled to room temperature, quenched with water 50 mL) and extracted with CH_2Cl_2 three times. The combined organic phase was washed with saturated sodium bicarbonate solution and water, then it was dried over anhydrous $MgSO_4$. The most of organic solvent was removed under reduced pressure and the residue was purified by silica gel column chromatography eluted with petroleum ether:CH_2Cl_2 (4:1, by volume) to obtain a white crystal as compound **1** (11.5 g, yield 68.9%). ^{1}H NMR ($CDCl_3$, 400 MHz, δ/ppm): 6.88 (s, 4H), 3.98 (t, 4H, J = 6.04 Hz), 1.81 (m, 4H), 1.57-1.28 (m, 20H), 0.88 (m, 6H).

*2.3.2. Synthesis of 1,2-bibromo-4,5-dioctyloxybenzene (**2**)*

Under Ar protection, to the mixture of compound **1** (9.5 g, 28.5 mmol), CH_3COOH (30 mL) and CH_2Cl_2 (100 mL) was slowly added Br_2 (3.3 mL, 62.5 mmol) diluted with 20 mL CH_2Cl_2. After

being stirring at room temperature for 4 h, the reaction mixture was quenched with water (50 mL) and extracted with CH_2Cl_2 three times. The combined organic phase was washed with sodium thiosulfate solution and brine, dried over anhydrous $MgSO_4$. The organic layer was evaporated under reduced pressure and the crude product subjected to silica gel column chromatography eluted with petroleum ether:CH_2Cl_2 (8:1, by volume) to obtain a white solid as compound **2** (10.3 g, yield 73.6%). ^{1}H NMR ($CDCl_3$, 400 MHz, δ/ppm): 7.05 (s, 2H), 3.93 (t, 4H, J = 6.04 Hz), 1.80 (m, 4H), 1.56-1.28 (m, 20H), 0.88 (m, 6H).

*2.3.3. Synthesis of 2,2'-(4,5-dioctyloxy-1,2-phenylene)dithiophene (**3**)*

To a degassed toluene (100 mL) solution of compound **2** (4.92 g, 10 mmol) was added 2-(tributylstannyl)thiophene (20.5 g, 50 mmol) and $Pd(PPh_3)_4$ (0.231 g, 0.2 mmol). The mixture was subjected to three freeze-pump-thaw cycles and was then stirred at 120 °C for 24 h. After cooling to room temperature, toluene was removed by evaporation to get black solid. The solid was dissolved into a little CH_2Cl_2 and then added into methanol (150 mL) to form a black solid. The crude product subjected to silica gel column chromatography eluted with petroleum ether:CH_2Cl_2 (10:1, by volume) to obtain a light green solid as compound **3** (2.17 g, yield 43.6%). ^{1}H NMR ($CDCl_3$, 400 MHz, δ/ppm): 7.23 (d, J = 7.60 Hz, 2H), 6.99 (s, 2H), 6.94 (t, J = 3.72 Hz, 2H), 6.83 (d, J = 2.50 Hz, 2H), 4.05 (t, J = 6.40 Hz, 4H), 1.85 (m, 4H), 1.59-1.28 (m, 20H), 0.88 (d, J = 7.70 Hz, 6H); MS (MALDI-TOF, *m/z*) calcd for $C_{30}H_{42}O_2S_2$: 498.263; found 498.328.

*2.3.4. Synthesis of 5,5'-(4,5-dioctyloxy-1,2-phenylene)bis(2,4-dibromothiophene) (**4**)*

Under Ar protection, compound **3** (1.99 g, 4.0 mmol), $CHCl_3$ (20 mL) and CH_3COOH (20 mL) was added into a 100 mL round bottom flask. Then NBS (3.2 g, 18 mmol) was added into the mixture in portions at the darkness. After being stirred at room temperature for 12 h, the reaction mixture was quenched with water (50 mL) and extracted with $CHCl_3$ three times. The combined organic phase was washed with sodium bicarbonate solution and brine, dried over anhydrous $MgSO_4$, and evaporated under reduced pressure. The crude product subjected to silica gel column chromatography eluted with petroleum ether:CH_2Cl_2 (6:1, by volume) to obtain a white solid as compound **4** (2.96 g, yield 91.4%). ^{1}H NMR ($CDCl_3$, 400 MHz, δ/ppm): 7.28 (s, 2H), 6.94 (s, 2H), 4.04 (t, J = 4.32 Hz, 4H), 1.84 (m, 4H), 1.57-1.30 (m, 20H), 0.89 (d, J = 4.36 Hz, 6H); MS (MALDI-TOF, *m/z*) calcd for $C_{30}H_{38}Br_4O_2S_2$: 813.901; found 814.016.

*2.3.5. Synthesis of 2,2'-(4,5-dioctyloxy-1,2-phenylene)bis(3-dibromothiophene) (**5**)*

Under Ar protection, compound **4** (1.22 g, 1.5 mmol) and THF (20 mL) was added into a 100 mL round bottom flask. Then *n*-BuLi (1.2 mL, 3 mmol) was added into the mixture dropwise at -78 °C. After being stirring for 0.5 h, methanol (0.5 mL) was added to quench and the reaction mixture was warmed to room temperature for stirring another 2 h. Water (20 mL) was added into the reaction mixture and then diethyl ether (50 mL) was added. The organic phase was washed with brine and water, dried over anhydrous $MgSO_4$, and evaporated under reduced pressure. The crude product subjected to silica gel column chromatography eluted with petroleum ether to obtain a white solid as compound **5** (818.9 mg, yield 83.3%). ^{1}H NMR ($CDCl_3$, 400 MHz, δ/ppm): 7.20 (d, J = 5.29 Hz, 2H), 7.02 (s, 2H), 6.92 (d, J = 5.20 Hz, 2H), 4.07 (t, J = 6.52 Hz, 4H), 1.89-1.82 (m, 4H), 1.48-1.17 (m, 16H), 0.88 (d, J = 6.60 Hz, 6H); MS (MALDI-TOF, *m/z*) calcd for $C_{30}H_{40}Br_2O_2S_2$: 656.082; found 656.068.

*2.3.6. Synthesis of 2,3-dioctyloxy-8-(p-tolyl)-8H-benzo[d]dithieno[3,2-b:2'3'-f]azepine (**6**)*

Under Ar protection, compound **5** (4.10 g, 6.25 mmol), *p*-toluidine (0.668 g, 6.25 mmol), $Pd_2(dba)_3$•$CHCl_3$, (312 mg, 5 mol%), (*t*-$Bu_3PH)BF_4$ (187.5 mg, 12 mol%), *t*-BuOK (1.75 g, 15.6 mmol) and toluene (60 mL) was added into a 100 mL round bottom flask. After mixing together, the mixture was stirred at 100 °C for 24 h. Then the reaction mixture was allowed to cool to room temperature, and it was filtered through a pad of celite and water (50 mL) was added. The filtrate was extracted with ethyl acetate three times. The combined organic phase was concentrated under reduced pressure and purified by column chromatography eluted with petroleum ether:CH_2Cl_2 (12:1, by volume) to obtain a light yellow solid as compound **6** (1.75 g, yield 46.5%). ^{1}H NMR ($CDCl_3$, 400 MHz, δ/ppm): 7.40 (d, J = 4.8 Hz, 2H), 7.10 (d, J = 4.80 Hz, 2H), 7.09 (s, 2H), 6.94 (*pseudo*-d, J = 8.40 Hz, 2H), 6.74 (*pseudo*-d, J = 8.40 Hz, 2H), 4.08 (t, J = 6.60 Hz, 4H), 2.24 (s, 3H), 1.87 (t, J = 7.20 Hz, 4H), 1.49-1.30 (m, 20H), 0.93 (t, J = 5.60 Hz, 6H); ^{13}C NMR (100 MHz, $CDCl_3$, δ/ppm): 148.85, 145.47, 141.73, 135.87, 129.39, 127.91, 127.70, 124.93, 123.93, 113.49, 112.34, 69.37, 31.88, 29.40, 29.34, 29.21, 26.06, 22.74, 20.34, 14.18. MS (MALDI-TOF, *m/z*) calcd for $C_{37}H_{47}NO_2S_2$: 601.305; found 601.333.

*2.3.7. Synthesis of 8-(p-tolyl)-2,3-dioctyloxy-6,10-diiodo-8H-benzo[d]dithieno[3,2-b:2'3'-f]azepine (**M1**)*

Under Ar protection, compound **6** (1.20 g, 2.0 mmol) and THF (20 mL) was added into a 100 mL round bottom flask. Then *n*-BuLi (1.83 mL, 4.4 mmol) was added into the mixture dropwise at

-40 °C. After addition of *n*-BuLi, the mixture was allowed to warm up room temperature and stirred for 1 h. Then the reaction mixture was cooling to -40 °C again and iodine (1.11 g, 4.4 mmol) was added. After being allowed to stir at room temperature for 12 h, the mixture was diluted with water (50 mL), exacted with diethyl ether and washed with saturated $Na_2S_2O_3$ and brine. The organic phase was dried over $MgSO_4$, evaporated under reduced pressure, and subjected to column chromatography eluted with petroleum ether:CH_2Cl_2 (10:1, by volume) to obtain a light yellow solid as compound **M1** (900.8 mg, yield 52.8%). ^{1}H NMR (400 MHz, $CDCl_3$, δ/ppm): 7.19 (s, 2H), 6.93 (s, 2H), 6.92 (*pseudo*-d, J = 8.00 Hz, 2H), 6.67 (*pseudo*-d, J = 8.00 Hz, 2H), 4.01 (t, J = 6.00 Hz, 4H), 2.21 (s, 3H), 1.82 (t, J = 6.00 Hz, 4H), 1.47-1.29 (m, 20H), 0.89 (t, J = 6.00 Hz, 6H); ^{13}C NMR (100 MHz, $CDCl_3$, δ/ppm): 149.22, 144.64, 141.69, 141.46, 136.85, 129.53, 128.54, 123.01, 112.95, 112.53, 72.93, 69.32, 31.91, 29.41, 29.37, 29.15, 26.05, 22.79, 20.43, 14.26. MS (MALDI-TOF, *m/z*) calcd for $C_{37}H_{45}I_2NO_2S_2$: 853.098; found 852.961.

*2.3.8. General synthetic procedure of D-A copolymers (for **PBTAPDPP** and **PBTAPBT**)*

These D-A copolymers were synthesized by Suzuki polycondensation. In a 25 mL two-neck flask, the dibromo BTAP monomer M1 (0.2 mmol, 1 equiv.), the bis(pinacolato)diboron comonomer (0.2 mmol, 1 equiv.), $Pd_2(dba)_3$ (9 mg), $P(o\text{-tyl})_3$ (15 mg), K_3PO_4 (848 mg, 4 mmol) and two drop of Aliquat 336 were subjected to three cycles of evacuation/argon purging, and then dissolved with 6 mL of degassed toluene after which 2 mL degassed water was added. The reaction mixture was stirred at 115 °C for 48 h under argon, and then cooled down to room temperature. The mixture was precipitated in 100 mL of methanol. The dark solids were filtered and Soxhlet extracted with methanol, acetone, hexane, and chloroform, successively. The chloroform extracts were concentrated and then subjected to column chromatography eluted with chloroform. The target polymer was afforded after completely drying in vacuo.

PBTAPDPP: The general Suzuki polymerization procedure was followed using 155.3 mg of monomer **M2** and 170 mg of monomer **M1** to afford a blue solid. (140.4 mg, yield: 62.6%). ^{1}H NMR (400 MHz, $CDCl_3$, δ/ppm): 9.01 (br, 2H), 7.36 (br, 3H), 7.06 (br, 4H), 6.79 (br, 3H), 4.06 (br, 8H), 2.21 (s, 3H), 1.84-1.28 (br, 42H), 0.92-0.91 (br, 18H). GPC: M_n: 67.2 kDa; PDI: 1.76.

PBTAPBT: The general Suzuki polymerization procedure was followed using 77 mg of monomer **M2** and 170 mg of monomer **M1** to afford a dark brown solid. (87.4 mg, yield: 57.3%). ^{1}H NMR (400 MHz, $CDCl_3$, δ/ppm): 8.25-8.23 (br, 2H), 7.89-7.86 (br, 2H), 7.19-7.17 (br, 2H),

7.02-6.85 (br, 4H), 4.07-4.05 (br, 4H), 2.21 (s, 3H), 1.84 (br, 4H), 1.48-1.29 (br, 20H), 0.88 (br, 6H). GPC: M_n: 7.7 kDa; PDI: 1.25.

*2.3.9. General synthetic procedure of D-D copolymers (for **PBTAPTh**, **PBTAPDTh**, and **PBTAPBDT**)*

Three D-D copolymers were synthesized by Stille polycondensation. In a 25 mL two-neck flask, the dibromo BTAP monomer **M1** (0.2 mmol, 1 equiv.), the bis(trimethylstannyl) comonomer (0.2 mmol, 1 equiv.), $Pd_2(dba)_3$ (9 mg) and P(*o*-tyl)$_3$ (15 mg) were subjected to three cycles of evacuation/argon purging, and then dissolved with 6 mL of degassed toluene. The reaction mixture was stirred at 115 °C for 48 h under argon, and then cooled down to room temperature. The mixture was precipitated in 100 mL of methanol. The dark solids were filtered and Soxhlet extracted with methanol, acetone, hexane, and chloroform, successively. The chloroform extracts were concentrated and then subjected to column chromatography eluted with chloroform. The target polymer was afforded after completely drying in vacuo.

PBTAPTh: The general Stille polymerization procedure was followed using 82 mg of monomer **M4** and 170 mg of monomer **M1** to afford a red solid. (97.3 mg, yield: 68.4%). ^{1}H NMR (400 MHz, $CDCl_3$, δ/ppm): 7.22-8.15 (br, 4H), 7.03-7.00 (br, 2H), 6.96-6.94 (br, 2H), 6.80-6.78 (br, 2H), 4.05 (br, 4H), 2.21 (s, 3H), 1.84 (br, 4H), 1.68-1.25 (br, 20H), 0.88 (br, 6H). GPC: M_n: 18.8 kDa; PDI: 1.33.

PBTAPDTh: The general Stille polymerization procedure was followed using 98.4 mg of monomer **M5** and 170 mg of monomer **M1** to afford a red solid. (93.5 mg, yield: 58.8%). ^{1}H NMR (400 MHz, $CDCl_3$, δ/ppm): 7.18-7.12 (br, 6H), 7.03-7.00 (br, 2H), 6.96-6.94 (br, 2H), 6.80-6.78 (br, 2H), 4.05 (br, 4H), 2.21 (s, 3H), 1.83 (br, 4H), 1.58-1.29 (br, 20H), 0.89 (br, 6H). GPC: M_n: 6.4 kDa; PDI: 1.42.

PBTAPBDT: The general Stille polymerization procedure was followed using 154.4 mg of monomer **M6** and 170 mg of monomer **M1** to afford a red solid. (135.6 mg, yield: 63.2%). ^{1}H NMR (400 MHz, $CDCl_3$, δ/ppm): 7.22-8.15 (br, 4H), 7.03-7.00 (br, 2H), 6.96-6.94 (br, 2H), 6.80-6.78 (br, 2H), 4.22 (br, 4H), 4.08 (br, 4H), 2.23 (s, 3H), 1.87-1.86 (br, 6H), 1.45-1.30 (br, 36H), 1.08-0.89 (m, 18H). GPC: M_n: 17.4 kDa; PDI: 1.38.

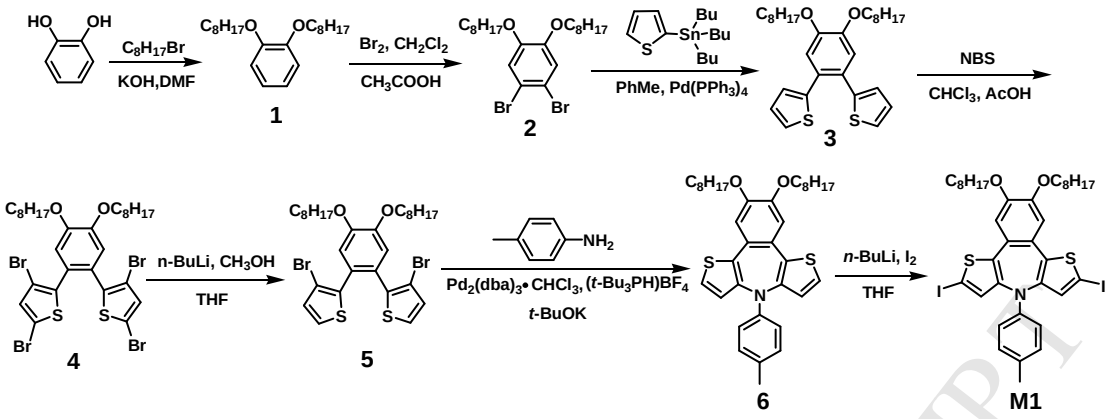

Scheme 2. Synthetic route of **BTAP**-based monomer **M1**.

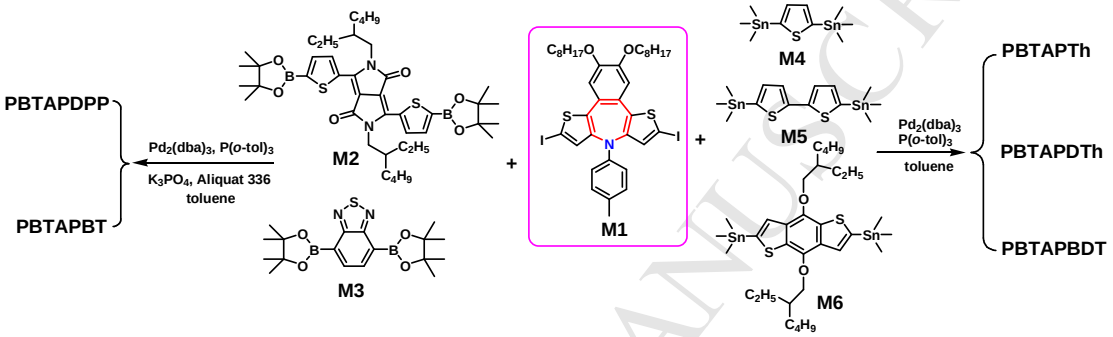

Scheme 3. Synthetic routes of **BTAP**-based D-D and D-A copolymers.

3. Results and discussion

3.1. Design, synthesis and characterization of the copolymers

The addition of annulation and steric effect has been proved as effective strategies to increase thermal and redox stability of heteroepines [20,21]. For nitrogen-containing azepine (**AP**, Chart 1), steric repulsion is unfavourable the norcaradiene intermediate. The molecule is thermally stable when bulky groups are introduced at the 2- and 7- positions. If aromatic rings are annulated to **AP**, a substantial resonance energy loss accompanies valence-isomerization. Therefore, our design of the stable **AP** building scaffold, named as benzo[*d*]-dithieno[3,2-*b*;2′,3′-*f*]azepine (**BTAP**), incorporates two thiophenes and one benzene ring (Chart 1). Thiophene ring is chosen as an annulation because of its intrinsically electrochemical stability and ease of synthetic modification through the *α*-position of the two annulated thiophenes (C6 and C10). In addition, two alkoxy groups can also be easily attached to the annulated benzene moiety to improve the solubility and π-π stacking of polymers based on **BTAP**, which is very important for efficient optoelectronic materials. Moreover,

N-alkylation of **BTAP** block can further control the solubility and the degree of planarity of molecules. Three electron-rich donor units and two electron-deficient acceptor building blocks were copolymerized with **BTAP** to construct D-D and D-A type copolymers with the aim to develop new **AP**-containing polymers and tailor the optoelectronic properties of the resulting materials.

Monomers **M2** and **M3** were directly purchased via commercial approach. Monomers **M4**-**M6** were synthesized according to the previously reported procedure [27]. **BTAP**-based monomer **M1** was prepared according to Swager's procedure with some modifications [21] and the corresponding synthetic route is depicted in Scheme 2. 1,2-Benzenediol was used as the starting material, that was easily converted into compound **1** through simple *O*-alkylation reaction. Compound **3** involving thiophene and benzene moieties was synthesized through a Stille coupling reaction between bromide **2** and 2-(tributylstannyl)thiophene with a moderate yield of 43.6%. Next, in order to introduce bromines into the 3- and 3'-positions, compound **3** was first subjected to bromination with NBS to form tetrabrominated compound **4**, and then debromination to achieve dibrominated compound **5**. This process has been proved to be necessary because bromination occurs at the 5-positions first, and moreover, lithium-bromine exchange also favors the less sterically hindered 5-positions. Then, the key intermediate of annulated azepine **6** was successfully synthesized via coupling dibromide **5** with *p*-toluidine using $Pd_2(dba)_3$•$CHCl_3$/(*t*-$Bu_3PH)BF_4$ catalyst system in an acceptable yield of 46.5%. Finally, the annulated azepine monomer **M1** was obtained as a light solid using a lithiation-iodine quenching sequence. The molecular structure of all newly synthesized compounds was characterized by ^{1}H NMR, ^{13}C NMR, and MS (MALDI-TOF) spectroscopies.

Five **BTAP**-based conjugated polymers were prepared by the palladium-catalyzed polycondensations of 6,10-diiodide monomer **M1** with functionalized electron-deficient (BT and DPP) or electron-rich (Th, DTh, and BDT) moieties, as described in Scheme 3. The polycondensations were carried out under Stille or Suzuki coupling conditions depending on the nature of comonomers, using $Pd_2(dba)_3$ as a catalyst and P(*o*-tyl)$_3$ as the corresponding ligand. Crude copolymers were first purified by extraction using methanol, acetone, hexane and chloroform, successively. The chloroform extracts were concentrated and then subjected to column chromatography eluted with chloroform to afford the resulting copolymers. The separated yields vary depending on the solubility of the polymers. Due to the lack of alkyl chains on the benzothiadiazole (BT) and dithiophene (DTh), **PBTAPBT** and **PBTAPDTh** exhibit relatively low

solubility and yields after Soxhlet extraction and column chromatography. The remainder of this study was carried out on materials out of the chloroform fractions, which have the higher molecular weights and not been further characterized. Molecular weights and polydispersity indices (PDIs) of polymers were determined through gel permeation chromatography (GPC) with THF as eluent against polystyrene standards. **PBTAPDPP**, **PBTAPTh**, and **PBTAPBDT** show relatively high number-average molecular weight (M_n) within 17.4-67.1 kDa, while the recorded M_n for **PBTAPBT** and **PBTAPDTh** suffers from poor solubility in THF for GPC analysis, leading to obvious lower M_n of 7.7 and 6.4 kDa, respectively. Notably, because the crude polymers subjected not only successive Soxhlet extraction but also column chromatography, all the polymers exhibit rather small PDIs varied from 1.33 to 1.76. The polymerization results and detailed GPC data are summarized in Table 1.

Table 1 Polymerization results and thermal properties of these polymers.

Polymer	yield (%)	M_n (kDa)[a]	M_w (kDa)[a]	PDI[a]	T_d (°C)[b]
PBTAPDPP	62.6	67.1	118.7	1.76	286
PBTAPBT	57.3	7.7	9.6	1.25	402
PBTAPTh	68.4	18.8	25.2	1.33	306
PBTAPDTh	58.8	6.4	9.1	1.42	392
PBTAPBDT	63.2	17.4	24.0	1.38	344

[a] Determined by GPC using polystyrene standards in THF. [b] The 5% weight loss temperatures under an inert atmosphere.

3.2. Thermal stability

Thermogravimetric analysis (TGA) was performed to investigate thermal stability of the copolymers, as shown in Fig. 1. All polymers demonstrate good thermal stability with the onset temperatures with 5% weight loss (T_d) above 300 °C except for **PBTAPDPP** with a T_d only 286 °C (see Table 1). The relatively lower T_d for **PBTAPDPP** should be ascribed to the slightly lower stability of DPP unit, which also has been observed in other previously reported DPP-based copolymers [29]. Obviously, the thermal stability of the copolymers is good enough for the applications in optoelectronic devices.

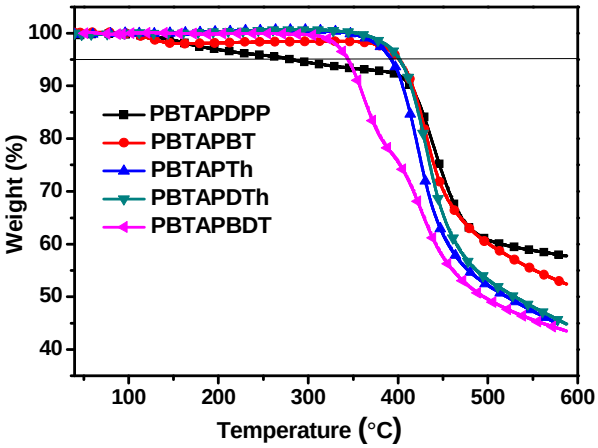

Fig. 1. TGA plots of the five copolymers at a heating rate of 20 °C min^{-1} under nitrogen.

3.3. Absorption spectra and optical bandgaps

The photophysical properties of the new polymers have been evaluated by UV-vis absorption both in dilute chloroform solution and as thin films (Fig. 2). The optical data including the absorption peak wavelength (λ_{max}), both in solution and films and optical bandgaps (E_g^{opt}) are summarized in Table 2.

As shown in Fig. 2a, two D-A copolymers **PBTAPDPP** and **PBTAPBT** exhibit obviously broader absorption spectra than those of three D-D copolymers **PBTAPTh**, **PBTAPDTh**, and **PBTAPBDT** in chloroform solution. This ascribes to the existence of intramolecular charge transfer (ICT) effect between the donor unit (**BTAP**) and acceptor unit (BT or DPP) in D-A type copolymer, resulting a low-energy absorption band at the range of 500-850 nm. In particular, **PBTAPDPP** shows a rather wide absorption extended to near-infrared region (> 800 nm) due to a stronger electron-deficient character of DPP unit. Moreover, one can see that the intensity of ICT for **PBTAPDPP** is higher than the π-π* transition of polymeric backbones located in the high-energy band (300-500 nm). However, for **PBTAPBT** the result is quite opposite (Fig. 2a). This difference should be due to the different electron-withdrawing strength of the two acceptors of BT and DPP. It is well known that the electron-withdrawing ability of DPP is stronger than BT, leading to an increase of the intensity of ICT absorption band and a remarkably red-shifted λ_{max} for **PBTAPDPP** as compared with **PBTAPBT**. Generally, the three D-D copolymers possess similar absorption profiles with narrow absorption bands ranged from 300-500 nm. The λ_{max} in solution of the copolymer **PBTAPTh** locates at about 435 nm. Compared with **PBTAPTh**, absorption

spectrum of **PBTAPDTh** displays a red shift by 13 nm (λ_{max} = 448 nm), and the absorption spectrum of **PBTAPBDT** further shifts to the red direction by about 20 nm (λ_{max} = 454 nm), which is probably due to the relatively long π-conjugation length of the BDT-based polymer main chains. The absorption spectra of these copolymers in films are displayed in Fig. 2b. The shape of the peaks and the trend of the absorption wavelength are generally similar to those of the polymer solutions. The λ_{max} of all the polymer films are red-shifted compared with those in solutions, which owes to the aggregation of the conjugated polymer main chains in the solid films. Furthermore, **PBTAPDPP** delivers a broad platform from 600 to 670 nm, meaning that there is a strong interchain interactions and good π-π stacking in polymer films.

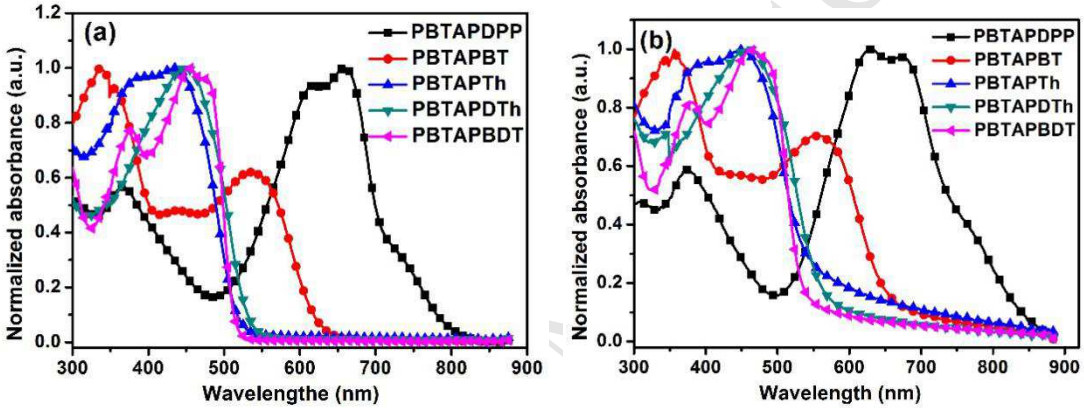

Fig. 2. Normalized UV-vis absorption spectra of the five polymers: (a) in chloroform solution; (b) as thin films.

The absorption onset (λ_{egde}) of the polymer film spectra are estimated to be 805, 625, 520, 534, and 513 nm for **PBTAPDPP**, **PBTAPBT**, **PBTAPTh**, **PBTAPDTh**, and **PBTAPBDT**, respectively, deducing an optical bandgaps (E_g^{opt}) of these polymers in the range of 1.54-2.42 eV (Table 2). Some conclusions can be deduced from these observations: (i) two D-A copolymers shows obviously smaller E_g^{opt} than those of D-D copolymers; (ii) due to the strong electron-withdrawing character of DPP unit, **PBTAPDPP** has a rather low bandgap of 1.54 eV, agreeing well with many of the reported D-A copolymers based on DPP unit [9]; (iii) the small difference between the three D-D copolymers indicates the three electron-donating building blocks, Th, DTh, and BDT, affect the bandgaps slightly; (iv) the large bandgap variations of **BTAP**-based polymers (1.54-2.42 eV) demonstrates that the optical bandgaps can be easily tailored to obtain different desired bandgaps, such as low-bandgap (**PBTAPDPP**), medium-bangdap (**PBTAPBT**)

and wide-bandgap (**PBTAPTh**, **PBTAPDTh**, and **PBTAPBDT**), by changing the electron-donating or electron-withdrawing character of a comonomer unit. More importantly, in view of easily tuned absorption region (300-900 nm), **BTAP**-based conjugated polymers could be used as efficient electron donor materials in fullerene or non-fullerene organic solar cells [30,31], especially their large bandgaps are supposed to be suitable for tandem heterojunction solar cells [32].

Table 2 Optical and electrochemical properties of the five copolymers.

Polymer	λ_{max} (nm)[a]	λ_{max} (nm)[b]	λ_{edge} (nm)[c]	E_g^{opt} (eV)[d]	E_{ox}/HOMO (V/eV)[e]	E_{red}/LUMO (V/eV)	E_g^{CV} (eV)
PBTAPDPP	659	629	805	1.54	0.75/-5.21	-0.94/-3.52[e]	1.69[g]
PBTAPBT	537	556	625	1.98	0.77/-5.23	-0.99/-3.47[e]	1.86[g]
PBTAPTh	435	450	520	2.39	0.75/-5.21	none/-2.82[f]	none
PBTAPDTh	448	461	534	2.32	0.74/-5.20	none/-2.88[f]	none
PBTAPBDT	454	463	513	2.42	0.91/-5.37	none/-2.95[f]	none

[a] Measured in dilute chloroform solution. [b] Measured on a quartz plate by polymers cast from chloroform solution. [c] The onset wavelength of the thin films. [d] Estimated from the onset wavelength of the absorption spectra: $E_g^{opt} = 1240/\lambda_{edge}$. [e] Calculated according to the equation: HOMO/LUMO = -e($E_{ox/red}$ + 4.46) (eV). [f] Calculated according to the equation: LUMO = E_g^{opt} + HOMO (eV). [g] Calculated according to the equation: E_g^{CV} = e($E_{ox} - E_{red}$) (eV).

3.4. Redox properties and molecular energy levels

Electrochemical cyclic voltammetry (CV) experiment was performed on thin films (spin-coated on indium tin oxide (ITO) substrates) of each polymer to study their redox properties. The CV curve was measured on a Pt electrode in a 0.1 M Bu_4NPF_6–acetonitrile solution and Ag/AgCl electrode as a reference that calibrated by the redox potential of a ferrocene/ferrocenium couple (Fc/Fc^+ measured as 0.34 V *vs* Ag/AgCl). Thus, the molecular energy levels (HOMO/LUMO) can be calculated from the following equation: HOMO/LUMO = e($E_{ox/red}$ + 4.46) (eV), where $E_{ox/red}$ is the oxidation/reduction onset potential of the polymers. Representative CVs of the five polymers including Fc/Fc^+ are displayed in Fig. 3 and the corresponding electrochemical properties are also recorded in Table 2.

As shown in Fig. 3a, two D-A copolymers give quasireversible oxidation waves and irreversible reduction waves. The E_{ox} and E_{red} values are observed to be 0.75/-0.94 and 0.77/-0.99 V for **PBTAPDPP** and **PBTAPBT**, respectively. Then, the HOMO/LUMO energy levels are calculated as -5.21/-3.52 eV for **PBTAPDPP** and -5.23/-3.47 eV for **PBTAPBT**. Whereas the three D-D copolymers just display quasireversible oxidation and no apparent reduction processes are observed from CV curves. Therefore, the resulted HOMO energy levels are deduced as -5.21, -5.20, and -5.37 eV for **PBTAPTh**, **PBTAPDTh**, and **PBTAPBDT** respectively, according to their relevant E_{ox} values (see Fig. 3b). Because the reduction potential onsets of the three D-D copolymers could not clearly be determined from the CVs (Fig. 3b), the LUMO energy levels of these polymers are estimated from the E_g^{opt} values and HOMO energy levels (LUMO = E_g^{opt} + HOMO) as measured by CV [18,29]. The electrochemical bandgaps (E_g^{CV}) are calculated to be 1.69 and 1.86 eV for **PBTAPDPP** and **PBTAPBT**, respectively, which are coincident with those of the corresponding E_g^{opt} (Table 2) of the polymer films within the reasonable range of deviation (0.2-0.5 eV) [33-36]. The electrochemical results reveal that all of these copolymers, except for **PBTAPBDT**, substantially have an almost identical HOMO energy level of about -5.21 eV, which is not surprising in view of the same **BTAP** donor moiety among all the copolymers [18]. Moreover, this series of **BTAP**-based polymers deliver the relatively low-lying HOMO energy levels (< -5.20 eV), implying good stability against oxidization in air [37], that would enhance device stability. Additionally, among these polymers **PBTAPBDT** has the lowest HOMO energy level of -5.39 eV, which would lead to a higher open-circuit voltage (V_{oc}) value for the solar cell with respect to the other four polymers since V_{oc} of the PSCs is presumed to proportionate to the difference between the HOMO level of the electron donor material and the LUMO level of the electron acceptor material [37]. On the other hand, the LUMO energy levels (see Table 2) of these polymers are found over a wide range: the LUMO level for **PBTAPDPP** is the deepest at -3.52 eV, while **PBTAPTh** has the highest at -2.82 eV. This implies that variation of the electron-related characteristic of comonomers has a great impact on the LUMOs of these **BTAP**-based polymers. Since these polymers will be intended to use as the donor material matching with a fullerene acceptor (i.e., $PC_{61}BM$ or $PC_{71}BM$), they should have LUMO and HOMO energy level offsets at least of 0.3 eV relative to $PC_{61}BM$ or $PC_{71}BM$ for the effective exciton dissociation and charge transfer [37-39]. To make a more clear comparison, a complete diagram of the HOMO/LUMO

energy levels of these polymers and $PC_{71}BM$ is presented in Fig. 4. From Fig. 4, one can find that the LUMO offsets and HOMO offsets between these polymers and $PC_{71}BM$ are large enough to meet the above mentioned requirements.

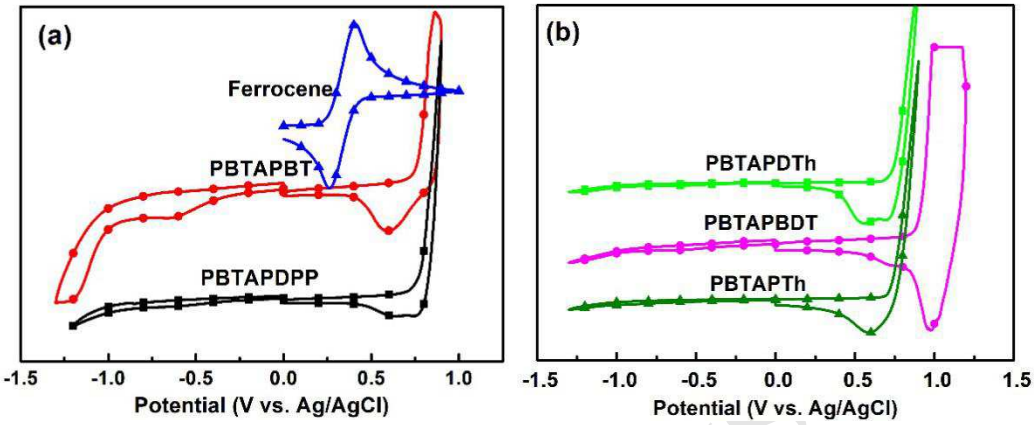

Fig. 3. Cyclic voltammograms of the polymer thin films on ITO glass electrode, recorded at a 100 mV s^{-1} scan rate in 0.1 M Bu_4NPF_6 acetonitrile solution: (a) **PBTAPDPP**, **PBTAPBT** and Ferrocene; (b) **PBTAPTh**, **PBTAPDTh** and **PBTAPBDT**.

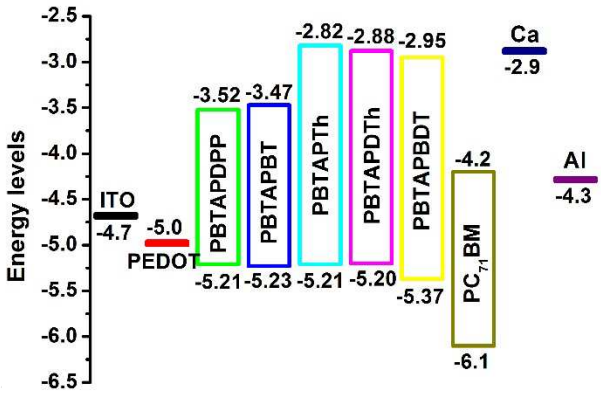

Fig. 4. Energy level diagrams of the five polymers and $PC_{71}BM$ using data derived from CV.

3.5. Photovoltaic properties

In consideration of the aforementioned features of the variable absorption and suitable molecular energy levels of the **BTAP**-based polymers, we assume that these polymers should be able to use as the effective electron donor materials in PSCs. Accordingly, BHJ type PSCs with the conventional device structure of ITO/PEDOT:PSS/polymer:PCBM ($PC_{61}BM$ or $PC_{71}BM$)/Ca/Al were fabricated to investigate the photovoltaic properties of the polymers. The photovoltaic data, such as open-circuit voltage (V_{oc}), short-circuit current density (J_{sc}), fill factor (FF), and power conversion

efficiency (PCE) are summarized in Tables 3 and 4. The typical current density-voltage (*J*-*V*) curves of the photovoltaic performance based on these polymers are described in Fig. 5.

First, we used $PC_{61}BM$ as the acceptor material combined with these polymers to prepare the photovoltaic device. When the blend ratio of polymer donor to $PC_{61}BM$ is determined to be 1:2 (by weight), the highest PCE of 0.51%, 0.34%, 0.25%, 0.38%, and 0.37% is obtained for **PBTAPDPP**, **PBTAPBT**, **PBTAPTh**, **PBTAPDTh**, and **PBTAPBDT**, respectively (see Table 3). Then, the acceptor is changed as $PC_{71}BM$, the photovoltaic performance is improved apparently, corresponding the best PCE up to 0.87% for **PBTAPDPP**, 0.93% for **PBTAPBT**, 0.58% for **PBTAPTh**, 0.82% for **PBTAPDTh**, and 1.00% for **PBTAPBDT**. The greatly enhanced PCEs mainly attribute to the substantial increase of J_{sc} values, as shown in Table 4. This is easily understood because $PC_{71}BM$ has the broader absorption spectrum compared to $PC_{61}BM$, which benefits the improvements of J_{sc} [40,41]. According to the data in Tables 3 and 4, one can find that no matter $PC_{61}BM$ or $PC_{71}BM$ as the acceptor, PSCs based on **PBTAPDPP** exhibit the highest J_{sc}, which accords with the relatively broader absorption (Fig. 2). On the other hand, **PBTAPBDT**-based PSCs deliver higher V_{oc} as compared with the other polymers, and moreover the highest V_{oc} of 0.84 V can be achieved after optimization of photovoltaic performance discussed in follow. This is because the V_{oc} of PSCs is tightly correlated with the energy difference between the HOMO level of a polymer donor and the LUMO level of an acceptor ($PC_{61}BM$ or $PC_{71}BM$) [37]. The polymer **PBTAPBDT** has the lowest HOMO energy level (see Table 2) and thus the PSCs containing this polymer displays the highest V_{oc}. Among these polymers **PBTAPBDT** possesses the best PCE, thus, we choose this polymer as a representative to further investigate the photovoltaic properties of these **BTAP**-based polymers. Previous studies have demonstrated that post-solvent treatment with a polar solvent can improve the photovoltaic performance of PSCs [42-49]. Here, methanol was chosen as a polar solvent to further optimize the photovoltaic performance of **PBTAPBDT**. As shown in Table 4, after the methanol treatment, the better photovoltaic performance is achieved with the highest PCE up to 1.28%, corresponding the significantly improved both of V_{oc} (0.84 V) and J_{sc} (5.20 mA cm^{-2}). Overall, the primary results indicate that **BTAP**-based polymer solar cells just can exhibit the moderate performance as a result of low J_{sc} and FF, which might be related to the charge mobility of the polymers and the morphology of the active layer.

Table 3 Photovoltaic properties of the PSCs based on these **BTAP**-based polymers with $PC_{61}BM$ as the acceptor.

polymer	V_{oc} (V)	J_{sc} (mA cm^{-2})	FF (%)	PCE (%)[a]
PBTAPDPP	0.78	2.37	27.7	0.51 (0.50±0.01)
PBTAPBT	0.75	1.70	27.0	0.34 (0.31±0.03)
PBTAPTh	0.62	1.35	29.4	0.25 (0.24±0.01)
PBTAPDTh	0.75	1.78	28.5	0.38 (0.35±0.03)
PBTAPBDT	0.79	1.65	28.8	0.37 (0.36±0.01)

[a] Average PCEs were obtained from more than 6 devices shown in parentheses.

Table 4 Photovoltaic properties and hole mobility of the PSCs based on these **BTAP**-based polymers with $PC_{71}BM$ as the acceptor.

polymer	V_{oc} (V)	J_{sc} (mA cm^{-2})	FF (%)	PCE (%)[a]	μ_h (cm^2 V^{-1} s^{-1})
PBTAPDPP	0.66	4.57	29.0	0.87 (0.86±0.01)	2.07×10^{-5}
PBTAPBT	0.72	4.30	29.8	0.93 (0.92±0.03)	2.33×10^{-5}
PBTAPTh	0.69	2.96	28.5	0.58 (0.57±0.01)	3.97×10^{-5}
PBTAPDTh	0.68	4.00	30.1	0.82 (0.80±0.02)	1.14×10^{-5}
PBTAPBDT	0.74	4.39	30.7	1.00 (0.98±0.02)	2.96×10^{-5}
PBTAPBDT[b]	0.84	5.20	29.4	1.28 (1.26±0.02)	-

[a] Average PCEs were obtained from more than 6 devices shown in parentheses. [b] Photovoltaic property treated with methanol.

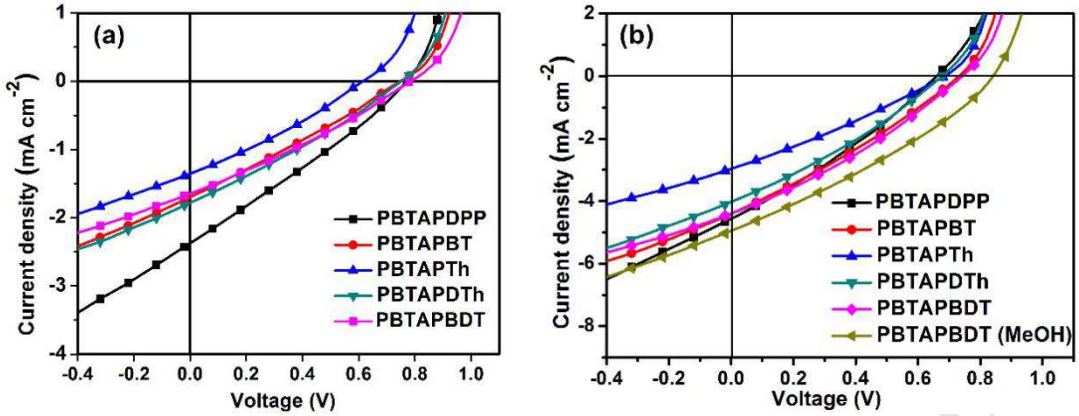

Fig. 5. Typical *J-V* curves of PSCs based on the five polymers: (a) with $PC_{61}BM$ as the acceptor; (b) with $PC_{71}BM$ as the acceptor.

3.6. Hole mobility

To search the possible reason resulted low performance of **BTAP**-based polymer solar cells, hole mobility (μ_h) of these polymers was measured because it is another important parameter for CPs using as donor materials in PSCs. To evaluate the charge mobility of these **BTAP**-based polymers, herein hole mobilities of these polymer:$PC_{71}BM$ blend film were measured by using the space-charge-limited current (SCLC) method with the hole-only device structure of ITO/PEDOT:PSS/polymer:$PC_{71}BM$/MoO_3/Al and estimated through the Mott–Gurney equation [50]. Fig. 6 displays the relationship between current and voltage in the hole-only devices of polymer:$PC_{71}BM$ blend films. The calculated hole mobilities are 2.07×10^{-5}, 2.33×10^{-5}, 3.97×10^{-5}, 1.14×10^{-5}, and 2.96×10^{-5} cm^2 V^{-1} s^{-1} for **PBTAPDPP**, **PBTAPBT**, **PBTAPTh**, **PBTAPDTh**, and **PBTAPBDT** blend film, respectively (see Table 4). Generally, the hole mobilities of all these **BTAP**-based polymers are relatively low as compared with other high-performance conjugated polymers [51-58]. Moreover, the μ_h value is much lower than electron mobilities of PCBMs ($\sim 10^{-3}$ cm^2 V^{-1} s^{-1}). The low and mismatch of charge mobilities should be partly responsible for the low J_{sc} and FF, and as a result that limits the performance of photovoltaic devices [59].

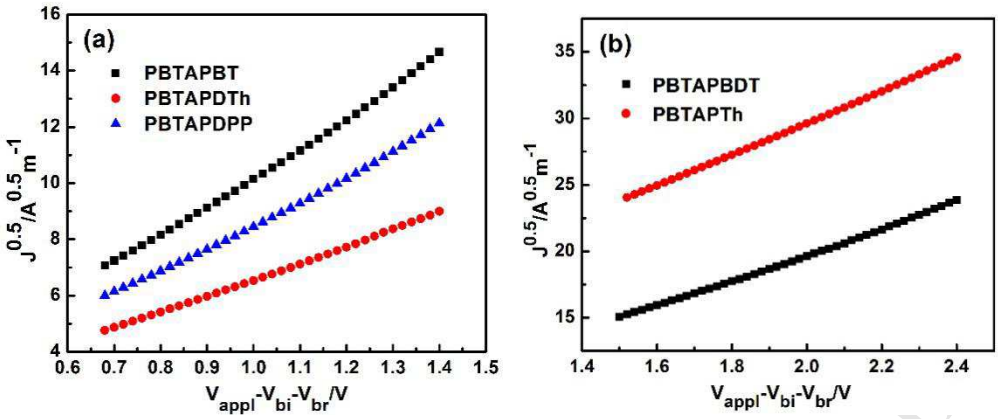

Fig. 6. $J_{1/2}$–V characteristics for the measurement of hole mobility in polymer:$PC_{71}BM$ devices by the SCLC method.

3.7. Morphology analyses of blend films

As we all know, the photovoltaic performance of the PSCs strongly depends on its morphological features. To seek the other reasons of the low J_{sc} and FF of these polymers, atomic force microscopy (AFM) is employed to study the morphology of the blend film. Among the five **BTAP**-based polymers, **PBTAPTh** and **PBTAPBDT** give the worst and best PCEs respectively, hence we have studied the morphology of the two polymer blend films. The AFM height and phase images of the blend films are described in Fig. 7. The height images of **PBTAPTh**:$PC_{71}BM$ (1:3 by weight, Fig. 7a) and **PBTAPBDT**:$PC_{71}BM$ (1:2 by weight, Fig. 7b) blend films reveal that both of these have rather smooth surfaces with a very small root-mean square roughness (R_q) of 0.470 and 0.881 nm, respectively. This observation indicates that the active layer has unobvious phase separation (see Figs. 7c and 7d), which is not good for the effective transport of charge carriers/collection and unfavorable to the production of high J_{sc} and FF. Additionally, **PBTAPBDT**:$PC_{71}BM$ blend film possesses a relatively rougher surface, meaning a relatively efficient exciton dissociation and transport of charge carriers and led to a higher J_{sc}. Furthermore, transmission electron microscopy (TEM) was performed to further investigate the composition and morphology of the polymer:$PC_{71}BM$ blends, as shown in Fig. 8. The blend films were prepared with a same condition to the optimized PSC devices. In the TEM images, the light and dark regions are assigned to polymer-rich and $PC_{71}BM$-rich domains, respectively. From Fig. 8, one can find that there is an unobvious polymer aggregation or $PC_{71}BM$ aggregation both in **PBTAPTh** and **PBTAPBDT** blends, implying a relatively excessive donor/acceptor compatibility for these two

blend films. Furthermore, this result shows that both of blends did not form regular interpenetrating network structure and desired nanoscaled phase separation, leading to a worse charge separation on the donor/acceptor interfaces. Overall, this non-ideal phase separation should be also responsible for the low J_{sc} to some extent.

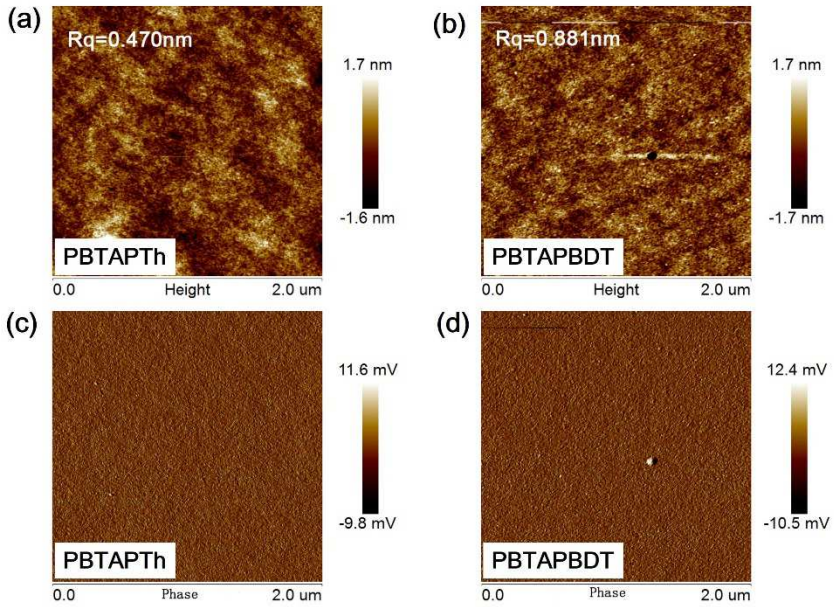

Fig. 7. AFM height (top) and phase (bottom) images of (a) and (c): **PBTAPTh**:$PC_{71}BM$ (1:3, by weight); (b) and (d): **PBTAPBDT**:$PC_{71}BM$ (1:2, by weight).

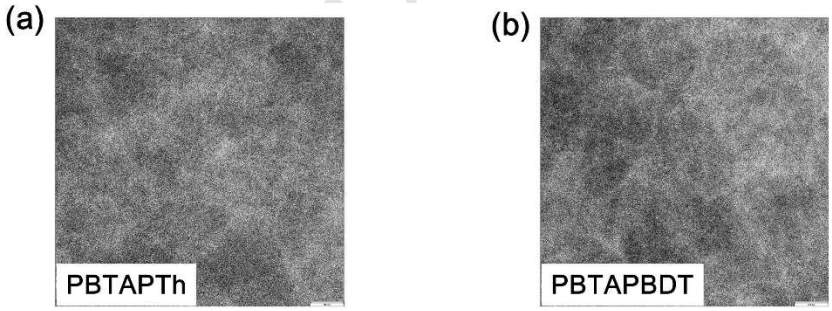

Fig. 8. TEM images of polymer:$PC_{71}BM$ blended films: (a) **PBTAPTh**:$PC_{71}BM$ (1:3, by weight); (b) **PBTAPBDT**:$PC_{71}BM$ (1:2, by weight). The scale bar in the TEM images is 200 nm.

4. Conclusions

In summary, a series of new conjugated polymers based on benzo[*d*]-dithieno[3,2-*b*;2′,3′-*f*]azepine (**BTAP**) were designed and synthesized by Stille or Suzuki cross-coupling reaction. Two electron-withdrawing aromatic copolymerization units (DPP and BT) and three electron-donating units (Th, DTh, and BDT) were employed to finely manipulate the

bandgaps and molecular energy levels of the resulting polymers. These polymers have good thermal and electrochemical stabilities. The polymers' absorption spectra can be effectively tuned throughout a wide range of 300-850 nm and the desired optical bandgaps between 1.54 and 2.42 eV are easily accessible depending on the electron-rich or electron-deficient character of comonomers. These polymers have nearly identical HOMO energy levels (~-5.21 eV) and various LUMO levels in the range of -2.82 ~ -3.52 eV. To expand the application fields of azepine-based conjugated polymers and tap the applied possibility in various organic electronic devices, BHJ type PSCs with these polymers as donors and PCBMs as acceptor were fabricated and characterized. Preliminary studies on PSCs based on these polymers deliver the highest PCE of 1.28% for **PBTAPBDT**-based solar cells with a relatively high V_{oc} of 0.84 V. The moderate performance of **BTAP**-based PSCs might attribute to low and unbalanced charge carrier mobility and non-ideal phase separation in polymer:PCBM blend films. Although photovoltaic performance of the solar cells based on these new polymers is still rather lower than the state of the art for fullerene-based PSCs (PCE > 10% [51,60-64]), to the best of our knowledge, this is the first report on synthesis and characterization of azepine-based conjugated polymers for application in organic electronic devices. Optimizations on molecular structures of polymers and morphologies of blend films for the further improvement of the photovoltaic performance are in progress. Our study open a new window for azepine containing polymers used as polymeric optoelectronic materials, such as PLEDs, PFETs, and photodetectors, which our future work is focusing on.

Acknowledgments

This work was supported by the National Natural Science Foundation of China (Grant no. 21574111), the Hunan 2011 Collaborative Innovation Center of Chemical Engineering & Technology with Environmental Benignity and Effective Resource Utilization and the Undergraduate Investigated-Study and Innovated Experiment Plan of Xiangtan University.

References

[1] H. Yao, L. Ye, H. Zhang, S. Li, S. Zhang, J. Hou, Molecular design of benzodithiophene-based organic photovoltaic materials, Chem. Rev. 116 (2016) 7397-7457.

[2] L. Lu, T. Zheng, Q. Wu, A.M. Schneider, D. Zhao, L. Yu, Recent advances in bulk heterojunction polymer solar cells. Chem. Rev. 115 (2015) 12666-12731.

[3] G. Li, R. Zhu, Y. Yang, Polymer solar cells. Nat. Photonics 6 (2012) 153-161.

[4] Z.-G. Zhang, Y. Li, Side-chain engineering of high-efficiency conjugated polymer photovoltaic materials, Sci. China Chem. 58 (2015) 192-209.

[5] L. Dou, Y. Liu, Z. Hong, G. Li, Y. Yang, Low-bandgap near-IR conjugated polymers/molecules for organic electronics, Chem. Rev. 115 (2015) 12633-12665.

[6] A.J. Heeger, Y. Cao, I.D. Parker, G. Yu, C. Zhang, Improved quantum efficiency for electroluminescence in semiconducting polymers, Nature 397 (1999) 414-417.

[7] H. Sasabe, J. Kido, Development of high performance OLEDs for general lighting, J. Mater. Chem. C 1 (2013) 1699-1707.

[8] C. Wang, H. Dong, W. Hu, Y. Liu, D. Zhu, Semiconducting π-conjugated systems in field-effect transistors: a material odyssey of organic electronics, Chem. Rev. 112 (2012) 2208-2267.

[9] Y. Li, P. Sonar, L. Murphya, W. Hong, High mobility diketopyrrolopyrrole (DPP)-based organic semiconductor materials for organic thin film transistors and photovoltaics, Energy Environ. Sci. 6 (2013) 1684-1710.

[10] Z. Yi, S. Wang, Y. Liu, Design of high-mobility diketopyrrolopyrrole-based π-conjugated copolymers for organic thin-film transistors. Adv. Mater. 27 (2015) 3589-3606.

[11] K.J. Baeg, M. Binda, D. Natali, M. Caironi, Y.Y. Noh, Organic light detectors: Photodiodes and phototransistors, Adv. Mater. 25 (2013) 4267-4295.

[12] D.S. Weiss, M. Abkowitz, Advances in organic photoconductor technology, Chem. Rev. 110 (2010) 479-526.

[13] S. Xiao, Q. Zhang, W. You, Molecular engineering of conjugated polymers for solar Cells: An updated report, Adv. Mater. 29 (2017) 1601391.

[14] L. Ye, H. Hu, M. Ghasemi, T. Wang, B.A. Collins, J.-H. Kim, K. Jiang, J.H. Carpenter, H. Li, Z. Li, T. McAfee, J. Zhao, X. Chen, J.L.Y. Lai, T. Ma, J.-L. Bredas, H. Yan, H. Ade, Quantitative relations between interaction parameter, miscibility and function in organic solar cells, Nat. Mater. 17 (2018) 253-260.

[15] L. Ye, B.A. Collins, X. Jiao, J. Zhao, H. Yan, H. Ade, Miscibility–function relations in organic solar cells: Significance of optimal miscibility in relation to percolation, Adv. Energy Mater. 8 (2018) 1703058.

[16] Y. Huang, E.J. Kramer, A.J. Heeger, G.C. Bazan, Bulk heterojunction solar cells: Morphology and performance relationships, Chem. Rev. 114 (2014) 7006-7043.

[17] J. Hou, M.-H. Park, S. Zhang, Y. Yao, L.-M. Chen, J.-H. Li, Y. Yang, Bandgap and molecular energy level control of conjugated polymer photovoltaic materials based on benzo[1,2-*b*:4,5-*b*′]dithiophene, Macromolecules 41 (2008) 6012-6018.

[18] P. Shen, X. Liu, P. Tang, B. Zhao, L. Wang, C. Weng, J. Cao, Y. Wu, Y. Chen, S. Tan, Bandgap and molecular-energy-level control of conjugated-polymer photovoltaic materials based on 6,12-dihydro-diindeno[1,2-b;10,20-e]pyrazine, Macromol. Chem. Phys. 214 (2013) 1147-1157.

[19] J.-S. Wu, S.-W. Cheng, Y.-J. Cheng, C.-S. Hsu, Donor-acceptor conjugated polymers based on multifused ladder-type arenes for organic solar cells, Chem. Soc. Rev. 44 (2015) 1113-1154.

[20] C. Song, T.M. Swager, Reactive conducting thiepin polymers, J. Org. Chem. 75 (2010) 999-1005.

[21] C. Song, D.B. Walker, T.M. Swager, Conducting thiophene-annulated azepine polymers, Macromolecules 43 (2010) 5233-5237.

[22] J.-M. Yang, C.-Z. Zhu, X.-Y. Tang, M. Shi, Rhodium(II)-catalyzed intramolecular annulation of 1-sulfonyl-1,2,3-triazoles with pyrrole and indole rings: Facile synthesis of *N*-bridgehead azepine skeletons, Angew. Chem. 126 (2014) 5242-5246.

[23] H.V. Kumar, N. Naik, Synthesis and antioxidant properties of some novel 5H-dibenz[*b*,*f*]azepine derivatives in different in vitro model systems, Eur. J. Med. Chem. 45 (2010) 2-10.

[24] D, He, L. Qian, L. Ding, A pentacyclic building block containing an azepine-2,7-dione moiety for polymer solar cells, Polym. Chem. 7 (2016) 2329-2332.

[25] J. Kim, T. Kim, S.Y. Bang, J. Kim, J.Y. Shim, I. Kim, S.Y. Park, H.H. Chun, J.Y. Kim, H. Suh, Syntheses and solar cell applications of conjugated copolymers consisting of 3,3′-dicarboximide and benzodithiophene units with thiophene and bithiophene linkage, Solar Energy Materials & Solar Cells 141 (2015) 24-31.

[26] C. Wang, J. Li, S. Cai, Z. Ning, D. Zhao, Q. Zhang, J.-H. Su, Performance improvement of dye-sensitizing solar cell by semi-rigid triarylamine-based donors, Dyes and Pigments 94 (2012) 40-48.

[27] P. Shen, H. Bin, L. Xiao, Y. Li, Enhancing photovoltaic performance of copolymers containing thiophene unit with D-A conjugated side chain by rational molecular design, Macromolecules 46 (2013) 9575-9586.

[28] P. Shen, Y. Tang, S. Jiang, H. Chen, X. Zheng, X. Wang, B. Zhao, S. Tan, Efficient triphenylamine-based dyes featuring dual-role carbazole, fluorene and spirobifluorene moieties, Org. Electron. 12 (2011) 125-135.

[29] M. Zhang, Y. Sun, X. Guo, C. Cui, Y. He, Y. Li, Synthesis and characterization of dioctyloxybenzo[1,2-*b*:4,3-*b*']-dithiophene-dontaining copolymers for polymer solar Cells, Macromolecules 44 (2011) 7625-7631.

[30] C.B. Nielsen, S. Holliday, H.-Y. Chen, S. J. Cryer, I. McCulloch, Non-fullerene electron acceptors for use in organic solar cells, Acc. Chem. Res. 48 (2015) 2803-2812

[31] W. Chen, Q, Zhang, Recent progress in non-fullerene small molecule acceptors in organic solar cells (OSCs), J. Mater. Chem. C 5 (2017) 1275-1302.

[32] O. Adebanjo, B. Vaagensmith, Q. Qiao, Double junction polymer solar cells, J. Mater. Chem. A 2 (2014) 10331-10349.

[33] P. Homyak, Y. Liu, F. Liu, T.P. Russel, E.B. Coughlin, Systematic variation of fluorinated diketopyrrolopyrrole low bandgap conjugated polymers: Synthesis by direct arylation polymerization and characterization and performance in organic photovoltaics and organic field-effect transistors, Macromolecules 48 (2015) 6978-6986.

[34] G. Liu, C. Weng, P. Yin, S. Tan, P. Shen, Impact of the number of fluorine atoms on crystalline, physicochemical and photovoltaic properties of low bandgap copolymers based on 1,4-dithienylphenylene and diketopyrrolopyrrole, Polymer 125 (2017) 217-226.

[35] X. Xu, Y. Wu, J. Fang, Z. Li, Z. Wang, Y. Li, Q. Peng, Side-chain engineering of benzodithiophene-fluorinated quinoxaline low-band-gap co-polymers for high-performance polymer solar cells, Chem. Eur. J. 20 (2014) 13259-13271.

[36] P.T. Wu, T. Bull, F.S. Kim, C.K. Luscombe, S.A. Jenekhe, Organometallic donor-acceptor conjugated polymer semiconductors: Tunable pptical, electrochemical, charge transport, and photovoltaic properties, Macromolecules 42 (2009) 671-681.

[37] M.C. Scharber, D. Mühbacher, M. Koppe, P. Denk, C. Waldauf, A.J. Heeger, C.J. Brabec, Design rules for donors in bulk-heterojunction solar cells—Towards 10% energy-conversion efficiency, Adv. Mater. 18 (2006) 789-794.

[38] C.J. Brabec, C. Winder, N.S. Sariciftci, J.C. Hummelen, A. Dhanabalan, P.A. van Hal, R.A.J. Janssen, A low-bandgap semiconducting polymer for photovoltaic devices and infrared emitting diodes, Adv. Funct. Mater 12 (2002) 709-712.

[39] L.J.A. Koster, V.D. Mihailetchi, P.W.M. Blom, Ultimate efficiency of polymer/fullerene bulk heterojunction solar cells, Appl. Phys. Lett. 88 (2006) 093511.

[40] R. Ganesamoorthy, G. Sathiyan, P. Sakthivel, Review: Fullerene based acceptors for efficient bulk heterojunction organic solar cell applications, Solar Energy Materials & Solar Cells 161 (2017) 102-148.

[41] Y. He, Y. Li, Fullerene derivative acceptors for high performance polymer solar cells, Phys. Chem. Chem. Phys. 13 (2011) 1970-1983.

[42] H. Bin, L. Xiao, Y. Liu, P. Shen, Y. Li, Effects of donor unit and π-bridge on photovoltaic properties of D-A copolymers based on benzo[1,2-*b*:4,5-*c*']-dithiophene-4,8-dione acceptor unit, J. Polym. Sci., Part A: Polym. Chem. 52 (2014) 1929-1940.

[43] Y. Wang, Y. Liu, S. Chen, R. Peng, Z. Ge, Significant enhancement of polymer solar cell performance via side-chain engineering and simple solvent treatment, Chem. Mater. 25 (2013) 3196-3204.

[44] L. Chen, P. Shen, Z.-G. Zhang, Y. Li, Side-chain engineering of benzodithiophene-thiophene copolymers with conjugated side chains containing the electron-withdrawing ethylrhodanine group, J. Mater. Chem. A 3 (2015) 12005-12015.

[45] X. Liu, W. Wen, G.C. Bazan, Post-deposition treatment of an arylated-carbazole conjugated polymer for solar cell fabrication, Adv. Mater. 24 (2012) 4505-4510.

[46] K. Kranthiraja, K. Gunasekar, W. Cho, M. Song, Y.G. Park, J.Y. Lee, Y. Shin, I.-N. Kang, A. Kim, H. Kim, B. Kim, S.-H. Jin, Alkoxyphenylthiophene linked benzodithiophene based

medium band gap polymers for organic photovoltaics: Efficiency improvement upon methanol treatment depends on the planarity of backbone, Macromolecules 47 (2014) 7060-7069.

[47] K. Kranthiraja, K. Gunasekar, W. Cho, Y.G. Park, J.Y. Lee, Y. Shin, I.-N. Kang, M. Song, K.H. Chae, B. Kimef, S.-H. Jin, Influential effects of π-spacers, alkyl side chains, and various processing conditions on the photovoltaic properties of alkylselenyl substituted benzodithiophene based polymers, J. Mater. Chem. C 3 (2015) 796-808.

[48] L. Ye, Y. Jing, X. Guo, H. Sun, S. Zhang, M. Zhang, L. Huo, J. Hou, Remove the residual additives toward enhanced efficiency with higher reproducibility in polymer solar cells, J. Phys. Chem. C 117 (2013) 14920-14928.

[49] H. Zhou, Y. Zhang, J. Seifter, S.D. Collins, C. Luo, G.C. Bazan, T.-Q. Nguyen, A.J. Heeger, High-efficiency polymer solar cells enhanced by solvent treatment, Adv. Mater. 25 (2013) 1646-1652.

[50] J. Mikroyannidis, P. Suresh, G. Sharma, Synthesis of a perylene bisimide with acetonaphthopyrazine dicarbonitrile terminal moieties for photovoltaic applications, Synth. Met. 160 (2010) 932-938.

[51] Z. Hu, L. Ying, F. Huang, Y. Cao, Towards a bright future: polymer solar cells with power conversion efficiencies over 10%, Sci. China Chem. 60 (2017) 571-582.

[52] C. Cui, W.Y. Wong, Y. Li, Improvement of open-circuit voltage and photovoltaic properties of 2D-conjugated polymers by alkylthio substitution, Energy Environ. Sci. 7 (2014) 2276-2284.

[53] L. Ye, S. Zhang, W. Zhao, H. Yao, J. Hou, Highly efficient 2D-conjugated benzodithiophene-based photovoltaic polymer with linear alkylthio side chain, Chem. Mater. 26 (2014) 3603-3605.

[54] Y. Liu, J. Zhao, Z. Li, C. Mu, W. Ma, H. Hu, K. Jiang, H Lin, H. Ade, H. Yan, Aggregation and morphology control enables multiple cases of high-efficiency polymer solar cells, Nat. Commun. 5 (2014) 5293-5301.

[55] Y. Jin, Z. Chen, S. Dong, N. Zheng, L. Ying, X.F. Jiang, F. Liu, F. Huang, Y. Cao, A novel naphtho [1,2-*c*: 5,6-*c*′] bis ([1, 2, 5] thiadiazole)-based narrow-bandgap π-conjugated polymer with power conversion efficiency over 10%, Adv Mater, 28 (2016) 9811-9818.

[56] K. Kawashima, T. Fukuhara, Y. Suda, Y. Suzuki, T. Koganezawa, H. Yoshida, H. Ohkita, I. Osaka, K. Takimiya, Implication of fluorine atom on electronic properties, ordering structures,

and photovoltaic performance in naphthobisthiadiazole-based semiconducting polymers, J. Am. Chem. Soc. 138 (2016) 10265-10275.

[57] V. Vohra, K. Kawashima, T. Kakara, T. Koganezawa, I. Osaka, K. Takimiya, H. Murata, Efficient inverted polymer solar cells employing favourable molecular orientation, Nat. Photonics 9 (2015) 403-408.

[58] B, Kan, M. Li, Q. Zhang, F. Liu, X. Wan, Y. Wang, W. Ni, G. Long, X. Yang, H. Feng, Y. Zuo, M. Zhang, F. Huang, Y. Cao, T.P. Russell, Y. Chen, A series of simple oligomer-like small molecules based on oligothiophenes for solution-processed solar cells with high efficiency, J. Am. Chem. Soc. 137 (2015) 3886-3893.

[59] C. Duan, C. Wang, S. Liu, F. Huang, C.H.W. Choy, Y. Cao, Two-dimensional like conjugated copolymers for high efficiency bulk-heterojunction solar cell application: Band gap and energy level engineering, Sci. China Chem. 4 (2011) 685-694.

[60] Z. Du, X. Bao, Y. Li, D. Liu, J. Wang, C. Yang, R. Wimmer, L.W. Städe, R. Yang, D. Yu, Balancing high open circuit voltage over 1.0 V and high short circuit current in benzodithiophene-based polymer solar cells with low energy loss: A synergistic effect of fluorination and alkylthiolation, Adv. Energy Mater. 7 (2017) 1701471.

[61] K. Feng, G. Yang, X. Xu, G. Zhang, H. Yan, O. Awartani, L. Ye, H. Ade, Y. Li, Q. Peng, High-performance wide bandgap copolymers using an EDOT modified benzodithiophene donor block with 10.11% efficiency, Adv. Energy Mater. 7 (2017) 1602773.

[62] I. Shin, H. Ahn, J.H. Yun, J.W. Jo, S. Park, S.-Y. Joe, J. Bang, H.J. Son, High-performance and uniform 1 cm^2 polymer solar cells with D1-A-D2-A-type random terpolymers, Adv. Energy Mater. 7 (2017) 1701405.

[63] J. Lee, D.H. Sin, B. Moon, J. Shin, H.G. Kim, M. Kim, K. Cho, Highly crystalline low-bandgap polymer nanowires towards high-performance thick-film organic solar cells exceeding 10% power conversion efficiency, Energy Environ. Sci. 10 (2017) 247-257.

[64] Jin, Y.; Chen, Z.; Dong, S.; Zheng, N.; Ying, L.; Jiang, X.-F.; Liu, F.; Huang, F.; Cao, Y. A novel naphtho[1,2-*c*:5,6-*c*′]bis([1,2,5]-thiadiazole)-based narrow-bandgap π-conjugated polymer with power conversion efficiency Over 10%, Adv. Mater. 28 (2016) 9811-9818.

Highlights

► A series of conjugated polymers based on benzodithienoazepine were developed.

►Optoelectronic properties can be easily tailored by varying the copolymerizing units.

► These polymers were characterized and firstly applied in organic photovoltaic field.

► PSCs based on the polymers showed an initial PCE of 1.28% with a high V_{oc} of 0.84 V.